Title

Using Buckling-Restrained Braces on Long-Span Bridges. II: Feasibility and Development of a Near-Fault Loading Protocol

Journal

Journal of Bridge Engineering, 21(5)

ISSN

1084-0702

Authors

Lanning, Joel

Benzoni, Gianmario

Uang, Chia-Ming

Publication Date

2016-05-01

DOI

10.1061/(asce)be.1943-5592.0000804

Using Buckling-Restrained Braces on Long-Span Bridges. II: Feasibility and Development of a Near-Fault Loading Protocol

Joel Lanning, P. E., M.ASCE[1]; Gianmario Benzoni[2]; and Chia-Ming Uang, M.ASCE[3]

Abstract: Buckling-restrained braces (BRBs) are reliable energy-dissipating axial members that recently became popular in the seismic design of buildings. Using the Vincent Thomas Bridge (VTB) as a case study, this research investigates the feasibility of using BRBs for seismic response mitigation of long-span bridges, especially those located adjacent to seismic faults. A satisfactory set of BRBs was identified through a parametric study using a finite-element model of the bridge. Simulated deformational demands on the BRB elements included loading features that are not reflected in current BRB design and testing provisions. Therefore, two new BRB loading protocols were developed for physical testing and prequalification. The simulated seismic response of the bridge was improved by using BRB parameters consistent with those that are commercially available. Therefore, the use of existing BRB technology was deemed feasible as a relatively maintenance-free seismic response mitigation system for long-span bridges near seismic faults. A companion paper discusses a testing program of full-scale BRBs subjected to these new protocols along with the implications for seismic-capacity-based design and testing procedures. DOI: 10.1061/(ASCE)BE.1943-5592.0000804. © *2016 American Society of Civil Engineers.*

Author keywords: Buckling-restrained braces; Long-span bridge; Near-fault; Loading protocol.

Introduction

The feasibility of using buckling-restrained braces (BRBs) on long-span bridges was investigated in response to an effort to identify options for a relatively maintenance-free seismic response mitigation system for the Vincent Thomas Bridge (VTB). Connecting San Pedro to Terminal Island and spanning the Palos Verdes Fault near Long Beach, California, the bridge is equipped with viscous-fluid dampers as part of a seismic retrofit completed in 1998. Fig. 1 provides an overall schematic of the bridge, including the location of the existing dampers and proposed BRBs between the side spans and cable bents (SC), the side span and towers (ST), and the main span and towers (MT). The dampers are intended to mitigate impacts between the suspended structure, the adjacent towers, and cable bents by damping their relative motion during significant seismic events (Moffat & Nichol Engineers 1996).

Recent Caltrans maintenance inspections revealed that the VTB devices incur unexpected internal wear due to ambient bridge motion. This wearing leads to loss of the viscous fluid, which in turn causes a gap in the hysteretic response (Benzoni et al. 2008). In this study, simulated bridge response predicts that impact is indeed avoided with fully effective dampers but is very likely to occur with damaged viscous dampers. Therefore, a replacement solution is sought to reduce the long-term maintenance costs of the bridge.

Background on the Use of BRBs

Although capable of achieving large values in cumulative ductility and dissipating large amounts of energy, BRBs are also relatively simple in construction and require little maintenance. They normally consist of a yielding steel core surrounded by, and decoupled from, concrete mortar within a hollow structural section, as shown in Fig. 2(a). These relatively new braces have rapidly gained popularity in the seismic design of buildings. Their rise in use is due in part to a comprehensive guide to the design of BRB frames (BRBFs) and a substantiated set of prequalifying testing criteria for BRBs developed by AISC and the Structural Engineers Association of California (AISC/SEAOC 2001; AISC 2005).

For BRBFs in buildings, the braces are permitted to yield and dissipate energy; at the brace, axial yield force is equal to

$$P_{ya} = A_c F_{ya} \quad (1)$$

where A_c = yielding core area; and F_{ya} = measured steel yield stress. Thus, per the seismic-capacity design philosophy, under large seismic forces the surrounding structure is permitted to remain elastic. Unlike conventional braces, BRBs exhibit larger forces in compression than in tension. The typical bilinear idealization of BRB hysteretic behavior and axial force cyclic overstrength factors, ν and $\beta\nu$, are shown in Fig. 2(b). The provisions of AISC 341 (AISC 2010) limit the compression-to-tension ratio $\delta\beta\Phi$ to a value of 1.3 as measured within the symmetric Protocol cycles of the prequalifying testing protocol (AISC protocol), which statistically represents the effects of far-field ground motion on building frames equipped with BRBs (Sabelli et al. 2003).

[1]Assistant Professor, Dept. of Civil and Environmental Engineering, California State Univ., Fullerton, CA 92834 (corresponding author). E-mail: joellanning@fullerton.edu

[2]Research Scientist, Dept. of Structural Engineering, Univ. of California, San Diego, La Jolla, CA 92093. E-mail: gbenzoni@ucsd.edu

[3]Professor, Dept. of Structural Engineering, Univ. of California, San Diego, La Jolla, CA 92093. E-mail: cuang@ucsd.edu

Note. This manuscript was submitted on July 24, 2014; approved on April 22, 2015; published online on January 20, 2016. Discussion period open until June 20, 2016; separate discussions must be submitted for individual papers. This paper is part of the *Journal of Bridge Engineering*,© ASCE, ISSN 1084-0702.

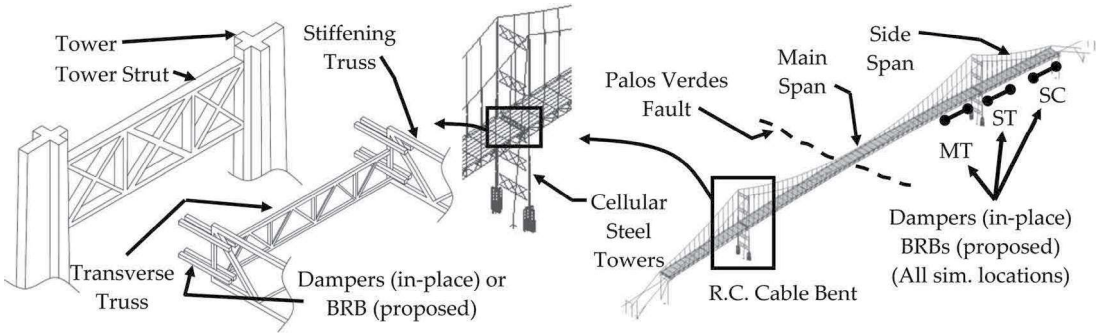

Fig. 1. VTB schematic and finite-element model (Note: sim. = similar)

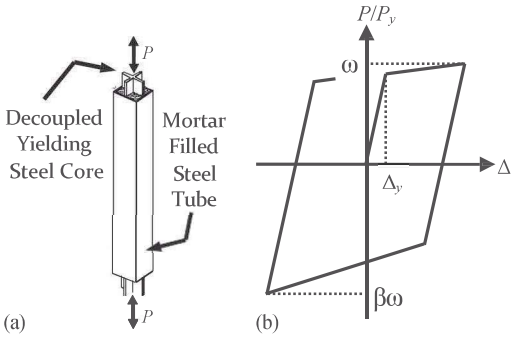

Fig. 2. (a) Typical BRB anatomy; (b) ideal hysteretic behavior and definition of cyclic overstrength factors ν and β

However, these braces are currently very uncommon in U.S. bridges and have no established design or testing procedures. Furthermore, there are no standards for addressing their use in near-fault situations. Given the complexity of long-span bridge structures and the lack of established bridge-specific BRB guidelines, finite-element simulation of the VTB seismic response was used to determine a feasible set of BRBs by varying the parameters that define the braces' primary characteristics. In this study, the BRBs were intended to replace the damaged viscous dampers. To be considered feasible for use, these BRBs were expected to provide enhanced seismic mitigation of the VTB while also being of practical proportions with respect to commercially available BRBs. Once a suitable BRB scheme was identified, it was obvious that the cyclic brace deformation demands were not reflected in the current AISC Protocol. Therefore, new protocols are needed to test the ability of BRBs to sustain the significantly different deformational demands imposed.

This article describes a parametric study performed to identify a set of feasible and beneficial BRBs for the VTB. With the use of the retrofitted bridge model, the development of two new loading protocols is presented. A near-fault protocol is proposed as a prequalifying test of BRBs for use on long-span bridges near seismic faults.

Identifying Proper BRB Characteristics through Parametric Variation

Finite-Element Modeling of the VTB

A seismic retrofit study performed in the mid-1990s was summarized in the *Caltrans Strategy Report for the Toll Road Seismic Retrofit Project for the Vincent Thomas Bridge* (Moffatt & Nichol Engineers 1996) and by Ingham et al. (1997). A major topic of these studies was the construction a sophisticated finite-element model of the VTB, shown in Fig. 1, which was used to justify the installation of the existing viscous dampers. Utilizing the nonlinear finite-element program *ADINA* (ADINA R&D 2003), the same model was used for this research. It is a well-established representation of the bridge, having been used in a number of different studies (e.g., Benzoni et al. 2008; He et al. 2008; Graziotti 2010). Throughout model development, and the studies mentioned, simulated modal properties and seismic responses have been reported to show good correlation to those extracted from ambient and earthquake-induced motions obtained from a system of accelerometers installed on the bridge in the 1980s.

Table 1. Periods of Vibration of VTB

Mode	Period (sec)	
	Damper model	Final BRB model
1	7.7	6.3
2	5.6	4.3
3	4.4	4.2

Note: See Fig. 3 for mode shapes.

The suspension system was modeled using tension-only three-dimensional (3D) linear elastic truss elements, which were prestrained during an initial gravity application analysis step, resulting in an as-constructed bridge geometry. The suspended spans, consisting of a concrete slab on a system of stringers and stiffening trusses, were represented using 3D linear elastic membrane and beam elements, respectively. Material nonlinearities were included in the tower structures, and various contact conditions were modeled with nonlinear elastic one-dimensional (1D) springs. The viscous dampers are characterized by use of spring and dashpot elements that provide the hysteretic response appropriate for linear viscous dampers, with element forces characterized by

$$P_D = Cv^1 \quad (2)$$

where C = damping constant; and v = relative velocity of the element ends. The dampers are oriented parallel to the bridge length corresponding with the first mode, as shown in Table 1 and Fig. 3, and the design motion fault-normal component. Similar configurations were used for the BRBs. In total, more than 20,000 degrees of freedom constituted the nonlinear finite-element model of the VTB (Moffat & Nichol Engineers 1996; Ingahm et al. 1998).

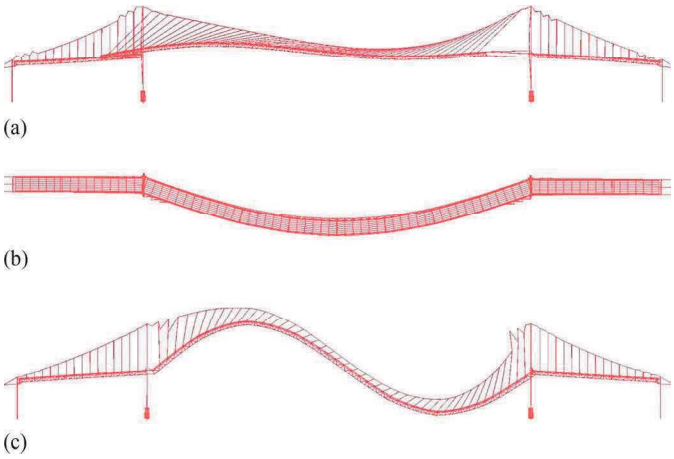

Fig. 3. Mode shapes of the VTB with dampers and with BRBs: (a) Mode 1—first longitudinal; (b) Mode 2—first transverse; (c) Mode 3—first vertical

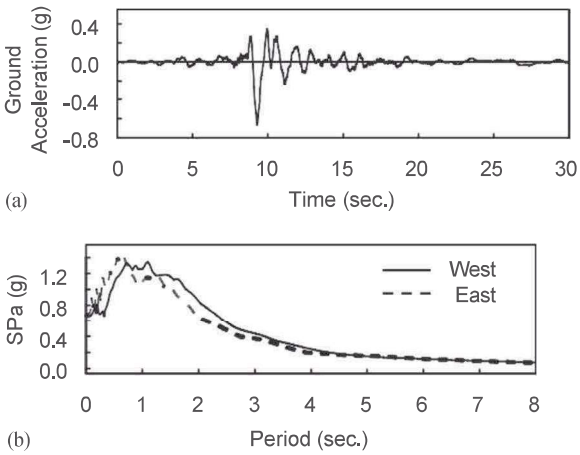

Fig. 4. VTB site-specific design-level earthquake bridge—longitudinal component: (a) west-side ground acceleration time history; (b) east and west elastic response spectra, 5% damping

Earthquake-Input Ground Motion

As part of the retrofit study, a site-specific seismic hazard and geotechnical parameter analysis led to the development of a set of design ground motions tailored to the VTB allowing for nonsynchronous multisupport shaking for seismic retrofit analyses. These ground motions represent an earthquake with approximately 2.3% probability of exceedance in 75 years. The seismic hazard of the design-level spectrum in the AASHTO *Guide Specifications for LRFD Seismic Bridge Design* (AASHTO 2011) is 7% in 75 years. The exposure, however, is based on an expected service life of a typical bridge, whereas that of the VTB was reported as 125 years in the *Caltrans Strategy Report* (Moffatt & Nichol Engineers 1996). Therefore, in terms of service life, the VTB design ground motion represents a 3.8% exceedance, which is considerably more severe than that of the AASHTO design spectrum. Because this design-level ground motion was developed specifically for the VTB site and represents significantly greater hazard than that given by AASHTO, it is considered to be the controlling motion for seismic demands on the structure.

The nonsynchronous set of ground motions was used for the retrofit summarized in the *Caltrans Strategy Report* (Moffatt & Nichol Engineers 1996), with each of the six modeled supports subjected to a 3D (fault-normal, fault-parallel, and vertical) ground excitation. A simplified approach was used in this study, with each side of the main span subjected to a set of 3D excitations, for a total of six excitations. A detailed discussion of the simplifications made was presented by Lanning et al. (2011). The east-side fault-normal component of ground acceleration, corresponding to the bridge longitudinal direction, and the east and west response spectra are shown in Fig. 4.

Finite-Element Modeling of the BRBs

A fairly common technique in the simulation of BRBs is the use of bilinear truss elements with kinematic hardening. The attributes of this element are displayed in Fig. 5(a) and consist of an elastic stiffness $\eth K_1\text{Þ}$, yield force $\eth P_y\text{Þ}$, postyield stiffness $\eth K_2\text{Þ}$, and kinematic cyclic hardening rule governing the translation of the yield surface. A direct comparison is provided in Fig. 5(b), which shows recent BRB testing data, collected by the authors, compared to those from the simulated response. Most notable is that this nonlinear truss element does not capture the Bauschinger effect, thereby underestimating the hysteretic energy, but overall, it sufficiently predicts the peak forces within the typical BRB testing range. BRBs in building frames were represented in this manner, with acceptable levels of error, by Black et al. (2004), Kim and Choi (2004), and Ravi et al. (2007). Usami et al. (2005) also utilized this model while studying the replacement of regular bracing of a steel arch bridge with energy-dissipating BRBs.

Parameterization of BRB Characteristics

Viscous damper elements at all six locations within the VTB model (see Fig. 1), were replaced by BRB elements. The primary characteristics of postyield stiffness, yield strength, and yielding core length were parameterized as described here and shown in Fig. 5(a) and (c).

To determine the sensitivity of the bridge response to the BRB postyield stiffness, the parameter was defined as

$$\alpha = \frac{K_2}{K_1} \tag{3}$$

where the elastic axial stiffness, $K_1 = \eth EA/L\text{Þ}$, is representative of the steel yielding core. The aforementioned studies exhibited α values ranging from 1.5% to 3.5%. The postyield slope value is necessary for use of the bilinear truss element to represent the BRB backbone curve for modeling cyclic response and is modeled as the slope between the yield point and a point on the measured hysteretic response. The particular postyield point depends on factors ranging from the expected maximum deformation to the type of steel material used for the yielding core. Therefore, α was explored in the 1–5% range because the maximum deformation was initially unknown.

Buildings with BRB frames typically rely on the equivalent lateral force procedure (ASCE 2010) to obtain initial brace yield forces. This method is not typically used in bridge designs, and the highly nonlinear suspension structure of the VTB is not well suited for this simplified method. Therefore, the brace yield force was investigated through the variation of

$$\gamma = \frac{P_y}{P_{u;D}} \tag{4}$$

where $P_{u;D}$ = the design axial capacity of the viscous dampers. For this study, BRB yielding cores were assumed to be of conventional A36 steel with an expected yield stress, F_{ye}, of 273 MPa

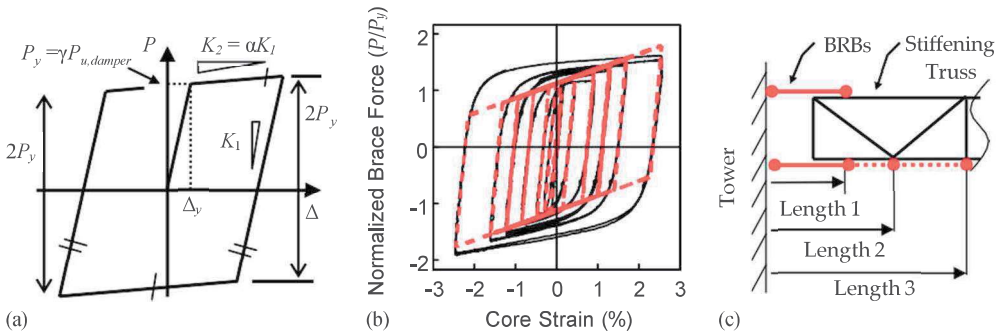

Fig. 5. (a) BRB bilinear truss element parameters; (b) comparison of BRB element with experimental results (reprinted from Lanning et al. 2012, with special permission from the BRB manufacturer); (c) BRB lengths considered in parametric study

(equal to 1.1 x 248 MPa) actual F_{ye}=F_{yn} ðequal to R_yÞ values from coupon tests conducted for prequalifying tests of BRBs, which are often less than the R_y ¼ 1:3 specified by AISC 2010. Normalizing the BRB yield force in this way facilitates a reference between the existing bridge construction and the proposed braces. The investigated range for BRB yield force was 0–200% of the damper's ultimate capacity (0%, indicating that no BRB is present).

Three brace configurations, defined as Lengths 1 through 3 (L1, L2, L3), are shown in Fig. 5(c). L1 represents a direct one-to-one BRB replacement of the dampers using the existing damper connection locations. L2 and L3 take advantage of the stiffening-truss geometry by assuming connections at the panel points. L3, also, somewhat corresponds to an upper bound to the feasible value, with an average core length of approximately 12.2 m among the three locations. Note that the BRB truss element represents only the yielding core length. The exposed ends of the core, which are very short, and the brace connections are designed to remain elastic through much larger cross-sectional areas, making their stiffness values much larger than those of the yielding core. Very often the yielding core is approximately 85% of the full brace stiffness. In this study, for simplicity, the length of the yielding core is assumed to be the same as the BRB length.

Monitored Response Quantities

Four peak response quantities were examined in the evaluation of each parameter combination. The peak displacement of each span toward its vertical support, or impact-direction displacement, was normalized by the displacement at which impact will occur. This parameter is represented by D_{IMP}. Thus, D_{IMP} ¼ 1 indicates that the simulated response predicts that the span will impact the vertical support; therefore, the smaller the value of D_{IMP}, the better the response mitigation. Responses obtained by various BRB configurations were also compared to those of the fully functioning dampers.

Three BRB demands were evaluated: peak core strain, peak brace force, and cumulative inelastic ductility (CID). Peak core strains of 4.3%, 4.7%, and 4.6% were successfully imposed on BRB specimens by Hasegawa et al. (1999), Carden et al. (2004), and Tremblay et al. (2006), respectively. Hence, this range was considered feasible, although uncommon, because most testing is conducted with the AISC protocol, which typically requires a peak core strain of only approximately 2%. Peak BRB force, P, normalized by $P_{u;D}$, was monitored as an indication of the peak-force demands imparted to the VTB structure. The AISC protocol requires a minimum achieved CID value of 200 times the yield deformation (i.e., the sum of the sustained inelastic strain, normalized by the yield deformation, must be at least 200). The CID from each BRB parameter combination was considered but is not presented here for brevity because the demands were always well within the measured CID capacities reported from many BRB testing studies (e.g., Merritt et al. 2003; Newell et al. 2006; Lanning et al. 2012).

Table 2. Seismic Responses of VTB with Viscous Dampers Resulting from the Design Earthquake

		Axial force	Displacement
Model with dampers	Damper location	P=$P_{u;D}$	D_{IMP}
Fully effective	SC	0.84	0.62
	ST	0.87	0.83
	MT	0.91	0.56
Fully ineffective	SC	—	0.75
	ST	—	1.47
	MT	—	1.09

Global Parametric Variation

The dynamic behavior of the bridge was modified by replacing the dampers, of theoretically no elastic stiffness, with the relatively stiff BRB elements. To gain a general understanding of the altered bridge behavior and the sensitivity to each parameter, the BRB properties were first applied and varied uniformly over the SC, ST, and MT locations. A reference point for the existing bridge response is provided in Table 2, which displays the D_{IMP} obtained from simulation using fully effective and fully ineffective dampers. Impact is predicted to occur with fully ineffective dampers at the ST and MT locations. Table 2 also reports the ratio of the peak axial force in the dampers to the damper design axial force as P=$P_{u;D}$. The fully effective damper values were used to evaluate the efficacy of each set of BRB parameters studied.

The postyield stiffness, α, from 1 to 5%, was varied for each of the three brace lengths, whereas γ was held constant at 0.70. The analyses showed bridge response to be insensitive to the value of α. It followed that an appropriate value to use was the range mean value, meaning α ¼ 3%. However, the bilinear truss element with α ¼ 3:25% provided a better prediction of peak forces and conservative levels of energy dissipation, as observed in many BRB experiments. The hysteretic response of the model is compared to one such BRB in Fig. 5(b). Therefore, α ¼ 3:25% was selected to remain constant for all BRBs for the remainder of the study.

The SC BRB results are presented in Fig. 6(a) as an example of the responses due to global variation of both γ and length (L1, L2, and L3). As might be expected, the impact-direction displacement

and peak core strain decreased with increasing γ and length values, and the MT BRB was the most sensitive location. However, core strain values with L1 fell far outside the feasible range in many cases, with some reaching beyond 10%. Peak axial forces increase with γ, but the SC BRB with L1 was the most extreme, reaching three times the $P_{u;D}$ value.

The observations from the global parameter study are summarized as follows:

1. The full range of yield force should be explored in a local parameter study, except γ ¼ 1:4, because the forces imparted to the structure increase rapidly with γ. Instead, the range was reduced to γ ¼ 2:5 so as not to excessively limit the parameter space.
2. L1 was eliminated due to unreasonably large core strains for many cases.
3. L3 provided lower strains, but the lengths approached unrealistic BRB core lengths and thus were eliminated.
4. Instead of continuing with only one length, two additional lengths were defined as those one-third and two-thirds between L2 and L3. Therefore, L2, L2.1, and L2.2 were used in local parameter studies.

Local Parametric Variation

Next, local parameter variation provided an understanding of the interaction between BRBs. First, each location considered γ from 0 to 1.25 (1.05 for ST), with the others held constant at 1.05. Promising cases were then studied further through the local variation of BRB length. Similarly, lengths were varied from L2 to L2.2, and the others were held constant at L2.

Fig. 6(b) shows that each span-to-support location exhibited impact with γ ¼ 0 (i.e., no BRB present). Relationships between each brace were observed as both impact-direction displacement and core strain increased at each location with increasing γ at the adjacent BRBs. The cases of γ ¼ 0:7; 1:05; and 1:25 for the SC BRB seemed promising because of the relatively low impact displacements, core strains within the acceptable range (;=4–5%), and reduced peak axial forces. These three γ values were therefore retained for length variation. The γ for ST BRB had a notable effect on the MT core strain, which was considered in the final parameter refinement. Only γ ¼ 1:05 was retained for length variation, however, because of the large impact-direction displacement or core strains with other yield forces. As in the global variation, the MT BRB was very sensitive to local change in γ. It is interesting to note that γ at this location had an evident effect on the impact displacement response of both side-span BRBs. The γ ¼ 1:05 and 1.25 cases were the most feasible, despite the increase at the ST location for γ ¼ 1:25.

The cases selected were then investigated considering different BRB lengths [Fig. 6(c)]. All response quantities stabilized to acceptable values for the SC BRB with γ ¼ 1:25 and L2.1; hence, this combination was selected as the suggested retrofit parameter for this location. The ST BRB clearly exhibited the best core strain with γ ¼ 1:05 and L2.2; all other responses were satisfactory. In addition, adjacent BRB demands were found to be insensitive to local refinement of SC and ST BRB lengths. The MT BRB presented two viable options: γ ¼ 1:05 with L2.1 and γ ¼ 1:25 with L2.2. Both options provided acceptable levels of axial core strain, and so their influence on the adjacent BRB demands were examined. In this case, little sensitivity was observed, and both impact displacement and core strain values were minimized at each location with MT γ ¼ 1:05 and L2.1. Therefore, this set of parameters was selected as the final combination suggested for retrofitting.

Results and Summary of the Parametric Study

BRB axial forces were moderately larger than those of the dampers. However, the net forces imparted to the towers were not severe because of the in-phase reactions of opposing ST and MT BRBs, as

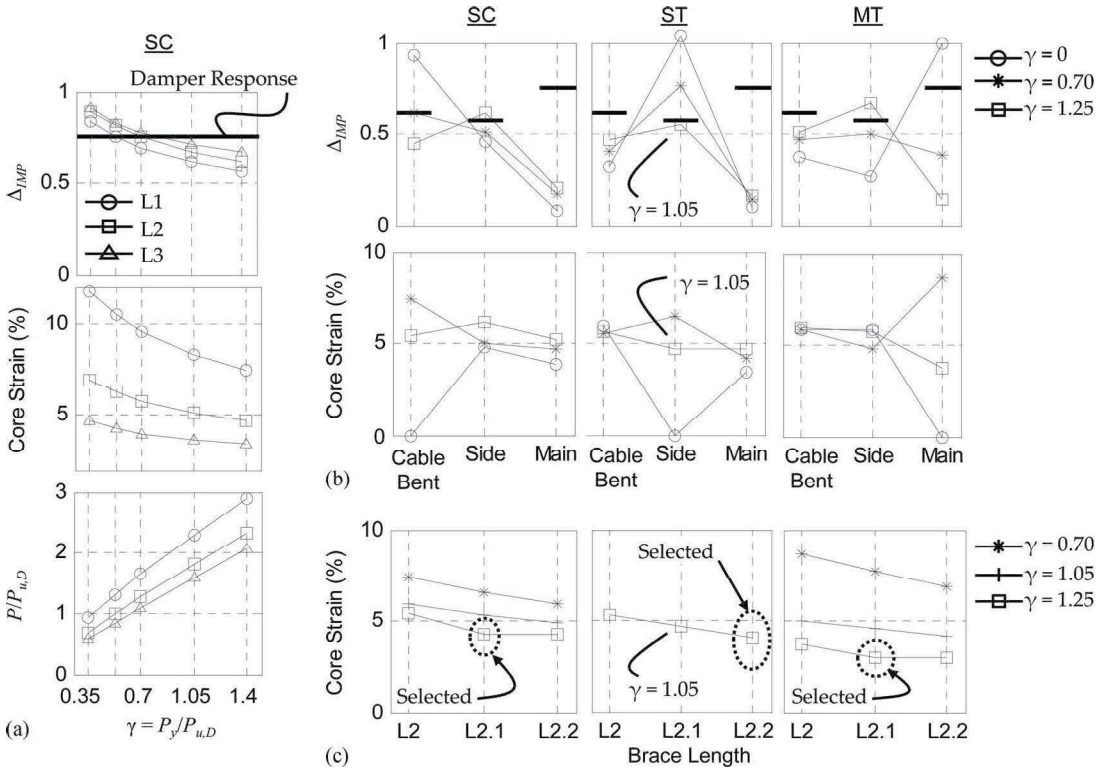

Fig. 6. Effects of parameter variation: (a) global BRB yield force and length; (b) local yield force; (c) refined local length

shown in Fig. 7. Conversely, damper forces were out of phase, which caused the net BRB increase over damper reaction forces to be only 33%, as calculated in Table 3. This effect caused the global tower longitudinal moment and shear to increase only modestly despite the larger individual axial forces of the BRBs.

The peak brace core strains were 4.4% on average (maximum, 4.9%) and occurred during one large deformation pulse corresponding to the ground motion pulse (Fig. 4). In addition, this deformation occurred over a very short time, causing the strain rate to be 16% s^{-1} (or 0.16 in./in./s), which is approximately 100 times faster than typical pseudostatic BRB testing rates (e.g., Merritt et al. 2003; Newell et al. 2006; Lanning et al. 2012). These maximum demands were observed in the SC BRB; the simulated hysteretic response is shown in Fig. 8(a).

The properties of the BRBs identified in the parametric study were within the range of those currently available commercially and were shown to provide significant seismic mitigation. Table 4 shows a summary of the final BRB parameter values, their physical meanings, and the improved simulated bridge response caused by the VTB design ground motion. All of these factors demonstrate BRBs to be a feasible seismic mitigation solution for long-span bridges near seismic faults. However, because the peak strain, strain rate, and unsymmetrical pulse excursions differ so much from the requirements of the AISC provisions, a new prequalifying loading protocol and testing program was required to confirm the ability of BRBs to sustain such deformations.

Development of Near-Fault Loading Protocols

Cyclic loading protocols for testing the seismic performance of structural components should assess the capability of surviving the statistically derived earthquake demands expected for a specific structure type and component configuration (Krawinkler et al. 1983), which is generally achieved by subjecting a number of representative structural models to a set of ground motions that constitute a certain level of seismic risk. The simulated component responses are collected and analyzed and then used to formulate a simplified, representative, and statistically significant demand time history. The resulting protocol should replicate a reasonably conservative cumulative damage estimate that is expected for the specific structural component (Krawinkler 1992).

The AISC protocol was developed in a similar manner, by using BRB deformations obtained from nonlinear time history analysis of several building frames equipped with BRBs (also modeled with bilinear truss elements) subjected to a suite of far-field ground motions (Sabelli et al. 2003). The AISC protocol (see Fig. 11) consists of symmetrical, gradually increasing amplitude cycles that typically reach a maximum core strain of approximately 2%.

Currently, there is no bridge-specific standardized BRB testing protocol or design procedure, and the effects of near-fault ground motion, including high strain rate, have been explicitly neglected for all structural systems in the AISC seismic provisions (AISC 2005, 2010). Therefore, the following sections describe the development of two protocols that are intended to provide reasonably conservative near-fault seismic demands for BRB testing; the second one is applicable for prequalification of BRBs for use on long-span bridges near seismic faults.

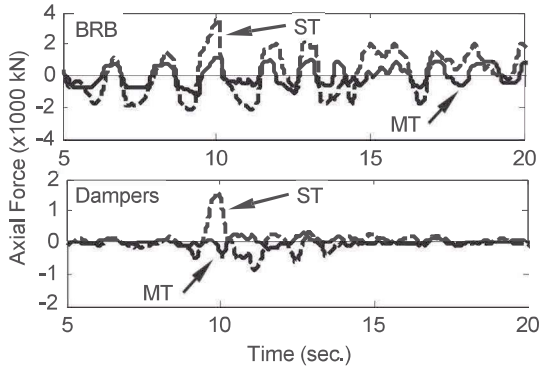

Fig. 7. BRB force phase relationship of BRBs and dampers on either side of a tower

Table 3. Net Increase of Device Axial Force Imparted to the Towers under Design Earthquake

BRB location	Peak axial force (kN)		% Increase BRB-to-damper
	In-phase BRB	Out-of-phase Damper	
MT	3,640	1,610	126
ST	1,200	−225	433
Net contribution	2,440	1,835	33

VTB Proof Protocol

Given the disparity between the deformation demands of the AISC protocol and the severe BRB demands from the simulated VTB design ground motion response, it was pertinent to develop a so-called proof protocol to serve as a key milestone to demonstrate that BRBs could sustain the 5% core strain pulse before more rigorous testing was conducted.

The SC BRBs, which exhibited the peak demands described earlier, were selected as the prototypical responses for the proof loading cycles. Inelastic cycles were placed in the order in which they occurred and assembled with increasing amplitudes leading up to the large pulse (two large excursions that cause the peak core strain). Amplitudes then decreased after the pulse and resulted in a

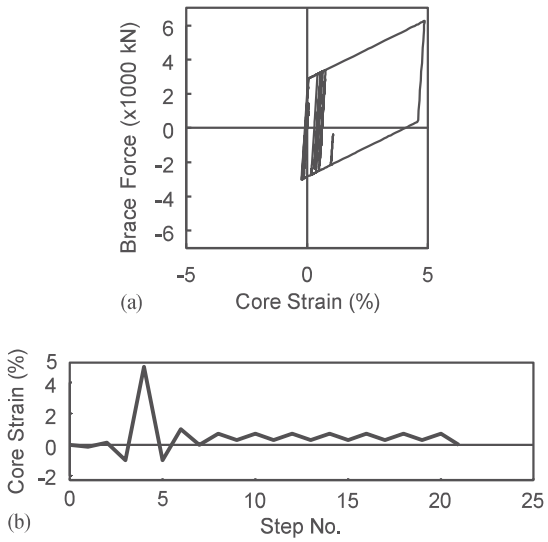

Fig. 8. VTB design ground motion results: (a) SC BRB hysteretic response with maximum peak strain; (b) the VTB proof protocol

Table 4. Final BRB Parameters for Effective VTB Retrofit and Resulting Response Reduction

	Final BRB properties								Design earthquake	
BRB location	g	Area (cm^2)	P_y (kN)	L	L_y (m)	a (%)	K_1 (kN/mm)[a]	K_2 (kN/mm)	Max strain (%)	Reduced displacement (%)
SC	1.25	107.7	2,950	2.1	10.4	3.25	208	7	25.4	4.9
ST	1.05	25.2	681	2.2	9.1		55	2	12.7	4.2
MT	1.05	68.4	1,868	2.2	9.4		140	5	58.1	4.1

[a]Corresponds to BRB yielding core stiffness.

Table 5. VTB Proof Protocol

Step number	Core strain (%)	Core strain Rate (% s^{-1})
1	−0.2	−0.2
2	0.2	1.6
3	−1.0	−5
4	5.0	16.2
5	−1.0	−7.2
6	1.0	3
7	0	−1.5
7 cycles	0.6 amplitude	1.4
Residual	0.6	

residual deformation. The VTB proof protocol is shown in Fig. 8(b) and summarized in Table 5.

Near-Fault Protocol

Because the VTB proof protocol considers only one ground motion, it is not appropriate for use as a prequalification test. Using the Pacific Earthquake Engineering Research Center Strong Motion Database (PEER), 17 near-fault pulse-type ground motions were scaled to the VTB design response spectrum (Fig. 4) up to a period of 6.5 s to cover the first-mode period (equal to 6:3 s) of the bridge in the longitudinal direction, as shown in Table 2. A summary of these motions and their respective scale factors is provided in Table 6.

These 17 ground motions and the VTB design earthquake were applied to the bridge finite-element model with the suggested BRBs, which resulted in a total of 54 brace deformation time histories (18 records × 3 locations), such as those shown in Fig. 9(a). The following loading characteristics were extracted for protocol development: (1) first- through fourth-largest-magnitude core strains, ε_{max}, $\varepsilon_{2;max}$, $\varepsilon_{3;max}$, and $\varepsilon_{4;max}$; (2) maximum inelastic strain excursion, $d\varepsilon_{max}$; (3) order of inelastic excursions, $d\varepsilon_i$; (4) residual strain, ε_R; and (5) number of inelastic excursions, N. The rainflow cycle counting algorithm (ASTM 2011), similar to that used by Krawinkler et al. (1983) and Richards and Uang (2006), was utilized to filter out elastic events, identify $d\varepsilon_{max}$, count N, and obtain the order in which each event occurred $(d\varepsilon_i)$. Each series of inelastic excursions was organized by aligning $d\varepsilon_{max}$, assumed to signify the pulse, thereby allowing the identification of the prepulse and postpulse excursions. An example of an aligned set of 18 inelastic excursions is shown in Fig. 9(b). At each step, the mean plus 1 SD of the magnitudes was calculated on the basis of the full number of records. Taking the statistical value in this way reduced the influence of excursions that occurred away from the pulse, in which every set may not have contained an inelastic event.

Cycles were formed as a sequence of core strains by summing the inelastic strain excursions by

$$\varepsilon(i) = \sum_{0}^{i} (-1)^{i} d\varepsilon_i \quad (5)$$

where $\varepsilon(i)$ is the ith peak strain; and $d\varepsilon_i$ is the ith excursion from each series. This process produced cycles forming a raw protocol, shown in Fig. 9(c), meaning that the core strain maxima and the residual strain are not necessarily represented. To incorporate them, only minor adjustments were required, as follows. First, the pulse cycles were defined as those that most nearly caused the four peak strain maxima that resulted from the alternating excursions in Eq. 4. Cycles within the pulse were amplified to attain the core strain maxima; however, the maximum excursion, $d\varepsilon_{max}$, was generally not affected significantly. Second, prepulse excursions were sorted such that the magnitudes increase, whereas postpulse cycles were sorted in descending order. Last, a few postpulse excursions were adjusted to result in the statistical residual strain, ε_R. All adjustments were minor and typically in the conservative direction, rounding up in strain or excursion magnitude. Fig. 9(c) compares the raw protocol to the final adjusted protocol, demonstrating the minor artificial adjustments made to the purely statistically obtained (raw) outcome.

This process was conducted for each BRB location, but the ST BRB resulted in the most severe loading sequence. A graphical summary of the demands obtained from each analysis at each BRB location is provided in Fig. 10 along with the final protocol demands, and the statistical values are organized in Table 7. The absolute maximum strain was selected to be 5%, in keeping with the proof protocol, rather than the mean plus 1 SD, over all three BRB locations; however, the value is still conservative over all three locations. All other parameters deviate only slightly from the mean plus 1 SD as a result of the minor adjustments described earlier.

The near-fault protocol is shown in Fig. 11(a), and Table 8 summarizes the core strains at each step. Fig. 11(a) and (b) together show the much smaller strains required by the AISC protocol. Fig. 11(c) demonstrates that the relative total cumulative inelastic ductility and the distribution of the ductility demand are much more severe. The near-fault protocol is proposed as a prequalifying test for BRBs intended for use on long-span bridges near seismic faults. However, it should be noted that only one bridge structure was used for its development. By including a variety of bridge models, the method presented could be applied to develop a bridge BRB prequalifying loading protocol for general use.

Dynamic Loading Protocols

Consideration of the strain-rate effect on structural steel components is often constrained to the increase in the yield and ultimate stresses

Table 6. Near-Fault Pulse-Type Ground Motions Used in VTB Protocol Development

Rec. number	Event	PGA[a] (g)	Epicenter distance (km)	Magnitude	Scale[b]
1	VTB design level	0.66	—	—	—
2	San Fernando (1971)	1.43	1.81	6.6	2.41
3	Cape Mendocino (1992)	1.27	6.96	7.0	2.51
4	Loma Prieta (1989)	0.94	3.88	6.9	1.34
5	Kobe (1995)	0.85	1.00	6.9	1.90
6	San Salvador (1986)	0.85	6.30	5.8	2.69
7	Northridge (1994)	0.84	5.19	6.7	1.61
8	Chi-Chi (1999)	0.82	0.60	7.6	1.20
9	Landers (1992)	0.72	2.19	7.3	2.84
10	Kobe (1995)	0.65	0.30	6.9	1.74
11	Chi-Chi (1999)	0.56	0.30	7.6	1.28
12	Erzikan, Turkey (1992)	0.49	4.40	6.7	1.92
13	Imperial Valley (1979)	0.46	0.56	6.5	1.87
14	Superstition Hills (1987)	0.42	0.95	6.5	1.66
15	Imperial Valley (1979)	0.38	0.07	6.5	2.30
16	Kocaeli, Turkey (1999)	0.36	6.60	7.5	1.76
17	Denali (2002)	0.33	2.70	7.9	1.62
18	Kocaeli, Turkey (1999)	0.28	4.80	7.5	2.09

[a]Peak ground acceleration before scaling.
[b]Scaled on the basis of response spectrum within period range of interest.

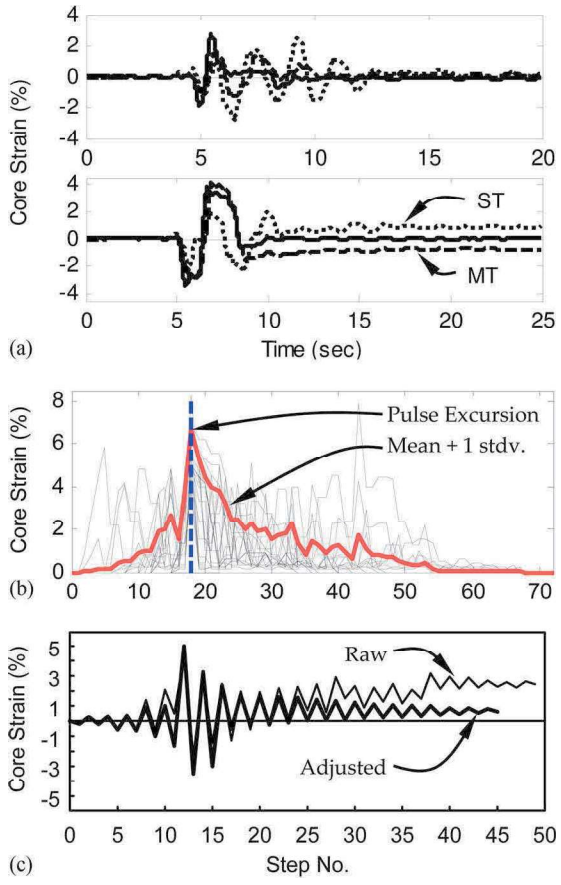

Fig. 9. Basic protocol development process: (a) example VTB BRB core strain time histories; (b) example of pulse-aligned inelastic excursions; (c) raw and adjusted near-fault protocol

under monotonic loading (e.g., Soroushian and Choi 1987). The increase is approximately 7% (Di Sarno et al. 2002), within the range of typical earthquake loading rates (approximately 1–10% s^{-1}), which is commonly considered to be negligible. In contrast, careful consideration is given to steel actual yield strength in capacity design. The AISC seismic provisions (AISC 2010) require nominal yield strength to be increased to reflect actual strength by the factor R_y, which can be as little as 1.10. In this light, it seems inconsistent to neglect the dynamic effect of roughly the same order.

Furthermore, the effect of strain rate on the cyclic response should also be considered. Dynamic cyclic material testing of A36 steel by Chang and Lee (1987) resulted in a cyclic stress increase of approximately 8% when constant-rate cycling was increased from 0.01 to 1% s^{-1}. High-strength carbon steel exhibited a hysteretic stress increase of approximately 5% when Chang et al. (2013) performed dynamic low-cycle fatigue tests at 0.1 and 100% s^{-1}. Both of these studies showed structural steel behavior to be independent of strain-rate history; varied strain rates during cycling resulted in hysteretic response, which stabilized to a stress level consistent with that of a cycle conducted at a constant rate. These results suggest that it may not be appropriate to neglect the dynamic cyclic effect for structural steel, even for strain rates attainable under earthquake loading, which is a conclusion shared by Chang and Lee (1987).

Cyclic testing of structural components is commonly performed at a pseudostatic rate, on the order of 0.01–0.1% s^{-1}, because of the limitations of many testing facilities. Following the convention of neglecting strain rate, these results are typically taken as an acceptable approximation. However, earthquake-induced strain-rate effects have been recognized to be of more importance for structural bracing undergoing inelastic buckling (Di Sarno et al. 2002). Moreover, this behavior could have a more significant influence on the constrained inelastic buckling condition of BRB yielding cores, in contrast to simple material tests as reported in the literature.

Fell et al. (2009) estimated earthquake loading rates for, and conducted testing of, steel special concentrically braced frames

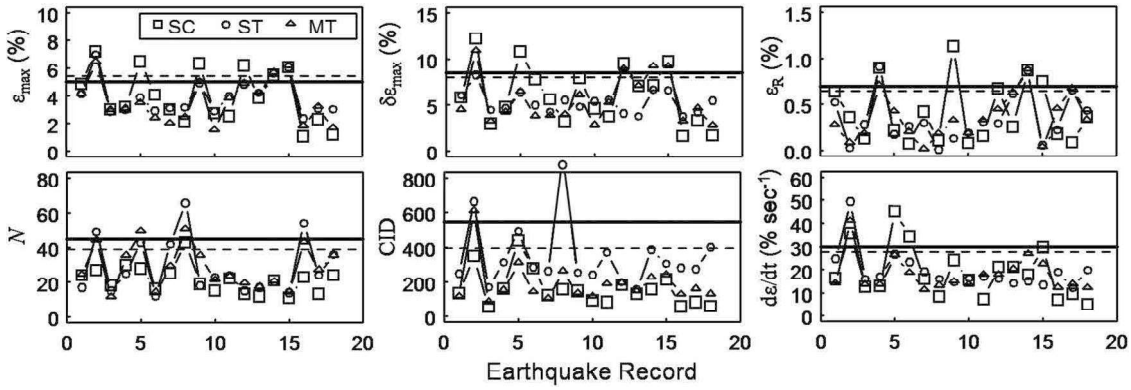

Fig. 10. Cyclic BRB demand quantities, 84th percentile (dashed line), and those represented by the near-fault protocol (solid line)

Table 7. Summary of Simulated and Near-Fault Protocol Cyclic Demand Parameters

		Simulated response				
Response parameter	BRB	Mean	s	Mean þ s	Near-fault protocol	AISC standard protocol
ε_{max} (%)	SC	4.0	1.9	5.8	5.00	2.00 (max)
	ST	3.9	1.3	5.2		
	MT	3.6	1.5	5.1		
$\varepsilon_{2;max}$ (%)	SC	2.7	1.7	4.4	3.50	1.50 (max)
	ST	2.9	1.6	4.0		
	MT	3.0	0.7	2.1		
$\varepsilon_{3;max}$ (%)	SC	2.4	0.8	3.7	3.25	1.00 (max)
	ST	2.7	0.8	3.		
	MT	3.0	0.8	3.5		
$\varepsilon_{4;max}$ (%)	SC	1.5	1.5	4.5	3.00	0.50 (max)
	ST	2.5	1.4	4.4		
	MT	2.3	1.2	3.5		
$d\varepsilon_{max}$ (%)	SC	6.1	3.1	9.1	8.50	4.00 (max)
	ST	5.3	1.2	6.4		
	MT	5.5	2.5	7.9		
ε_R (%)	SC	0.4	0.3	0.7	0.70	0
	ST	0.4	0.3	0.6		
	MT	0.4	0.2	0.6		
N	SC	21.3	7.7	29.0	45	25 (min)
	ST	28.6	15.5	44.0		
	MT	28.3	12.0	40.3		
Dissipated energy (10^3 kN-m)	SC	6.68	4.19	10.87	21.7	8.4 (min)
	ST	4.08	1.75	5.86	5.4	1.7 (min)
	MT	4.50	2.79	7.29	13.1	4.7 (min)
CID ðxD_yÞ	SC	161	101	262	524	200 (min)
	ST	347	185	532	545	
	MT	188	117	305	545	
Strain rate (% s^{-1})	SC	18.9	11.2	30.0	30.0	0.1 to 0.2 (typical)
	ST	19.5	8.4	27.9		
	MT	17.8	7.5	25.2		

resulting in a maximum strain rate of 5% s^{-1}, which represents a strain rate approximately 100 times faster than typical pseudostatic rates (assuming an average 0.05% s^{-1}) and 5 times faster than the tests of A36 steel reported earlier. Few studies are available in the literature that incorporated deliberate dynamic versus pseudostatic testing of BRBs. Carden et al. (2004) performed dynamic tests on short BRBs, within ductile end frames of bridge spans, under a constant frequency of 2 Hz, resulting in a maximum core strain rate of approximately 14% s^{-1}. Tremblay et al. (2006) subjected BRBs to dynamic loading with a maximum rate of approximately 25% s^{-1}. These cases were reported to have increased BRB hysteretic forces by 15% and 5%, respectively, compared to similar pseudostatically loaded braces.

Table 9 displays the rates from several standard BRB prequalification testing programs, those from available testing programs that were conducted at higher rates, and those of the simulated VTB BRB responses. In addition, Dehghani and Tremblay (2012) recently developed standard dynamic loading protocols for BRBFs considering Canadian seismic hazards that contain a maximum of approximately 3% s^{-1}; however, no physical testing was reported. In each of these cases, peak core strains, strain rates, or both are much smaller than those of the simulated VTB BRB responses.

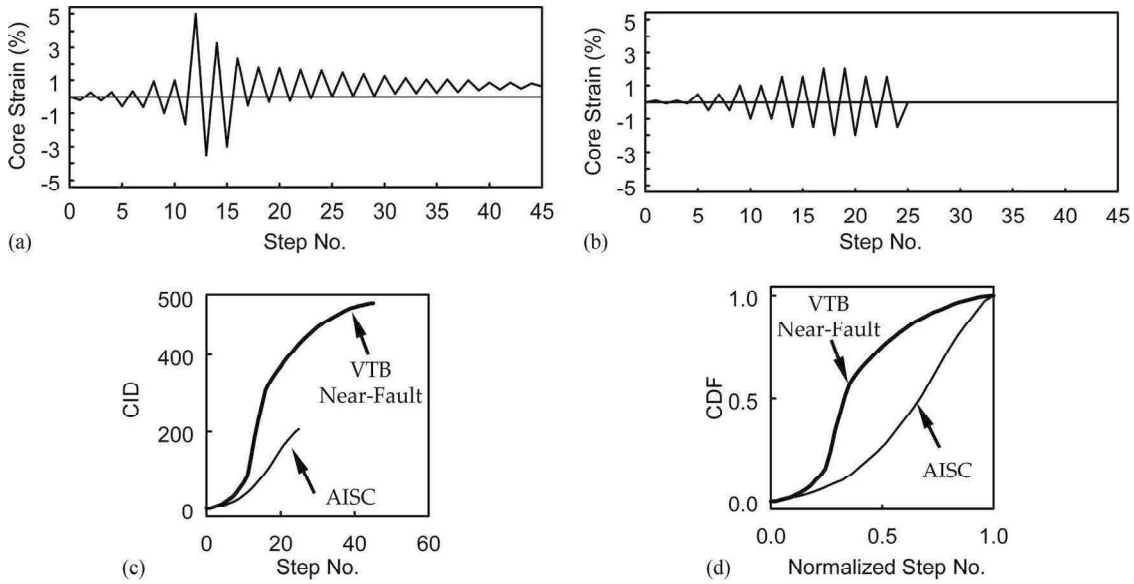

Fig. 11. (a) Proposed near-fault loading protocol; (b) AISC standard loading protocol; (c) relative CID demand; (d) cumulative distribution

Therefore, dynamic versions of the VTB protocols were developed to investigate the strain-rate effect on BRB performance.

Development of Dynamic Near-Fault Protocols

Pseudostatic protocols consist primarily of peak deformations organized in a particular order, or step, as indicated on the horizontal axis of Fig. 11(a). The conversion of pseudostatic VTB protocols to dynamic obviously requires the incorporation of time rather than only loading step. For a pseudostatic rate of 0.2% s^{-1}, the time step can be nearly uniform, but for the dynamic protocols, a series of compatible sine waves was used with an adjusted time step to reflect the appropriate wave periods resulting in the target strain rate. Smooth velocity and acceleration time histories were also ensured to accommodate the operation of testing equipment.

The simulated VTB BRB strain-rate histories followed similar trends as the core strains and excursion magnitudes; in general, the rate increased leading up to the pulse excursions and decreased thereafter, with the peak rate usually corresponding with the peak strain (i.e., the excursions forming the peak strain contained the peak rate). In forming the dynamic VTB proof and near-fault protocols, only the mean-plus-1-SD peak strain-rate values of 16% and 30% s^{-1} were explicitly included, respectively, which corresponded to a time step scaling within the pulse excursions by approximately 150 (30=0:2), and 80 (16=0:2) times faster than pseudostatic time step. The prepulse and postpulse cycles were adjusted to result in increasing strain rates leading to the pulse and decreasing rates afterward. The dynamic near-fault protocol is shown in Fig. 12, with the strain rates provided in Table 8, and those of the dynamic proof protocol are shown in Table 5.

Summary and Conclusions

The feasibility of using BRBs on long-span bridges was demonstrated through a parametric case study of the VTB, which spans a seismic fault. This case study was conducted in response to an effort to determine a maintenance-free seismic response mitigation system for the bridge. The properties of the identified BRBs were within the range of those that are current commercially available and provided significant bridge seismic response mitigation. Table 4 presents the final BRB parameters along with their physical meanings and the reduction in span-to-support relative displacement.

The near-fault pulse-type design earthquake used in the study required much more severe BRB deformation demands than those required by the current prequalifying testing protocol given by AISC 341 (AISC 2010). Therefore, two new loading protocols were developed with the simulated BRB demands due to these ground excitations applied to the long-span VTB model. A suite of 18 such ground motions was used to form the near-fault loading protocol based on the mean plus 1 SD of the inelastic cyclic demands from the analyses. In addition, the simulated strain rates were observed to be more than 2 orders of magnitude higher than typical pseudostatic BRB testing rates. Hence, dynamic versions of the proof and near-fault protocols were also developed, which incorporated the simulated peak strain rates of 16% and 30% s^{-1}, respectively. Table 8 summarizes the core strains and rates of both versions of the near-fault protocol.

These statistically representative loading sequences can be utilized for subsequent BRB physical testing to verify the ability of commercially available braces to sustain the demands of long-span bridges at risk of large near-fault ground motion. Furthermore, the dynamic versions of these protocols can be used to investigate the dynamic response of BRBs. It should be noted, however, that these protocols were developed with responses from a single bridge structure. Future developments of a BRB prequalifying loading protocol for general use should consider BRB demands obtained from multiple bridge models.

Acknowledgments

Funding for this research was provided by the California Department of Transportation under Contract Number 65A0358, with Dr. Charly Sikorsky as the project manager. The authors also acknowledge Lian Duan, Richard Heninger, Don Lee, and Li-Hong Sheng for providing advice during this project.

Table 8. Near-Fault Protocol

Step number	Core strain %	Core strain Rate (% s^{-1})
1	−0.2	−0.5
2	0.3	0.9
3	−0.2	−2.5
4	0.3	2.4
5	−0.6	−2.8
6	0.4	4.3
7	−0.6	−9.4
8	0.9	9.5
9	−1.0	−13.3
10	1.0	13.7
11	−1.7	−18.4
12	5.0	30.1
13	−3.5	−30.4
14	3.3	30.8
15	−3.0	−20.5
16	2.4	17.1
17	−0.5	−14.4
18	1.7	12.7
19	−0.3	−11.3
20	1.7	11.3
21	−0.3	−11.3
22	1.6	11.2
23	−0.1	−6.6
24	1.6	6.6
25	0.0	−6.6
26	1.4	7.2
27	0.1	−3.6
28	1.3	3.6
29	0.1	−3.6
30	1.2	4.4
31	0.2	−1.6
32	1.1	1.4
33	0.2	−1.4
34	1.1	1.4
35	0.3	−1.4
36	1.0	1.4
37	0.3	−1.4
38	1.0	1.4
39	0.4	−1.4
40	0.9	1.4
41	0.5	−1.4
42	0.9	1.4
43	0.5	−1.4
44	0.8	1.4
45	0.6	−1.4

Table 9. BRB Testing Strain Rates

Source	Protocol	Max strain %	Max strain Rate (% s^{-1})
Romero et al. 2007	AISC 2005	1.7	6×10^{-3}
Merritt et al. 2003	AISC/SEAOC 2001	1.7	0.1
Newell et al. 2006	AISC 2005	1.7	0.3
Lanning et al. 2012	AISC 2010	1.7	0.2
Merritt et al. 2003	Real-time, 1994 Northridge, Sylmar	3.1	9.0
Carden et al. 2004	Reverse, AISC/SEAOC 2001	1.9	23.9
	Real time, 1995 Kobe	4.7	Not reported
Tremblay et al. 2006	Dynamic BRBF Protocol (Tremblay and Bouatay 2002)	1.3	11.6
Simulated VTB demand	Design level	4.9	16.2
	Suite of 18 records	7.2	50.0
VTB dynamic proof protocol		5.0	16.0
VTB dynamic near-fault protocol		5.0	30.0

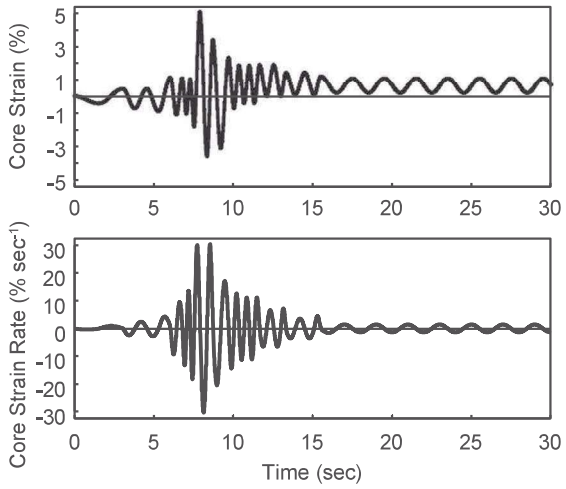

Fig. 12. Dynamic version of the proposed near-fault protocol

Notation

The following symbols are used in this paper:

A ¼ BRB finite-element area;
A_c ¼ yielding core area;
C ¼ viscous damper damping constant;
E ¼ BRB finite-element steel Young's modulus;
F_{ya} ¼ measured steel yield stress;
K_1 ¼ BRB finite-element elastic stiffness;
K_2 ¼ BRB finite-element postyield stiffness;
N ¼ number of inelastic excursions;
P ¼ BRB axial force;
P_y ¼ BRB finite-element yield force;
P_{ya} ¼ actual brace yield force;
P_D ¼ viscous damper force;
$P_{u;D}$ ¼ viscous damper design axial force capacity;
v ¼ relative velocity of viscous damper ends;
α ¼ parameterized postyield stiffness, ratio of K_2 to K_1;
β ¼ compression strength adjustment factor;
D ¼ BRB deformation;
D_{IMP} ¼ normalized bridge span impact-direction displacement;
D_y ¼ BRB yield deformation;
$\delta\varepsilon_i$ ¼ ith inelastic strain excursion;
$\delta\varepsilon_{max}$ ¼ maximum inelastic strain excursion;
ε_{max} ¼ maximum inelastic strain;
$\varepsilon_{i;max}$ ¼ secondary inelastic strain maxima;
ε_R ¼ residual inelastic strain;

ε_i = ith inelastic strain;

γ = parameterized yield force, ratio of P_y to $P_{u;D}$; and

ν = tension strength adjustment factor.

References

AASHTO. (2011). "Guide specifications for LRFD seismic bridge design." *LRFDSEIS-2*, Washington, DC.

ADINA R&D. (2003). *Automatic dynamic incremental nonlinear analysis.* ADINA R&D, Watertown, MA.

AISC. (2005). "Seismic provisions for structural steel buildings." *AISC 341-05*, Chicago.

AISC. (2010). "Seismic provisions for structural steel buildings." *AISC 341-10*, Chicago.

AISC/SEAOC. (Structural Engineers Association of California). (2001). Recommended provisions for buckling-restrained braced frames, Chicago.

ASCE. (2010). "Minimum design loads for buildings and other structures." *ASCE 7-10*, Reston, VA.

ASTM. (2011). "Standard Practices for Cycle Counting in Fatigue Analysis." *E1049*, West Conshohocken, PA.

Benzoni, G., Amaddeo, C., DiCesare, A., and Palermo, G. (2008). "A damage identification procedure for bridge structures with energy dissipation devices." *Rep. No. SRMD-2007/08*, Dept. of Structural Engineering, Univ. of California, San Diego, La Jolla, CA.

Black, C., Makris, N., and Aiken, D. (2004). "Component testing, seismic evaluation and characterization of buckling-restrained braces." *J. Struct. Eng.*, 10.1061/(ASCE)0733-9445(2004)130:6(880), 880–894.

Carden, L., Itani, A., Buckle, I., and Aiken, I. (2004). "Buckling restrained braces for ductile end cross frames in steel plate girder bridges." *Proc., 13th World Conf. on Earthquake Eng.*, Vancouver, BC, Canada, Paper No. 503.

Chang, K. C., and Lee, G. (1987). "Strain rate effect on structural steel under cyclic loading." *J. Eng. Mech.*, 10.1061/(ASCE)0733-9399(1987)113:9(1292), 1292–1301.

Chang, K. H., Jang, G. C., Stiemer, S., and Loewen, N. (2013). "Dynamic hysteretic characteristics of high-strength steels (POSTEN60, POSTEN80) and application of dynamic hysteresis model to FE analysis." *J. Mater. Civ. Eng.*, 10.1061/(ASCE)MT.1943-5533.0000629, 1549–1557.

Dehghani, M., and Tremblay, R. (2012). "Standard dynamic loading protocols for seismic qualification of BRBFs in eastern and western Canada." *Proc., 15th World Conf. on Earthquake Eng.*, Lisbon, Portugal.

Di Sarno, L., Elnashai, A. S., and Nethercot, D. A. (2002). "Comparison between seismic response characteristics of carbon steel and stainless steel." *Proc., 12th European Conf. on Earthquake Eng.*, Elsevier, Oxford, U.K., Paper No. 765.

Fell, B., Kanvinde, A., Deierlein, G., and Myers, A. (2009). "Experimental investigation of inelastic cyclic buckling and fracture of steel braces." *J. Struct. Eng.*, 10.1061/(ASCE)0733-9445(2009)135:1(19), 19–32.

Graziotti, F. (2010). "Seismic bridge response modification due to degradation of viscous dampers." M.Sc. thesis, Dept. of Structural Engineering, Univ. of California, San Diego, La Jolla, CA.

Hasegawa, H., Takeuchi, T., Iwata, M., Yamada, S., and Akiyama, H. (1999). "Dynamic performances of unbonded braces." *AIJ Tech. Rep. No. 9*, Architectural Institute of Japan, Tokyo, 103–106 (in Japanese).

He, X., Moaveni, B., Conte, J. P., Elgamal, A., and Masri, S. F. (2008). "Modal identification study of Vincent Thomas Bridge using simulated wind-induced ambient vibration data." *Comput.-Aided Civ. Infrastruct. Eng.*, 23(5), 373–388.

Ingham, T. J., Rodriguez, S., and Nader, M. (1997). "Nonlinear analysis of the Vincent Thomas Bridge for seismic retrofit." *Comput. Struct.*, 64(5–6), 1221–1238.

Kim, J., and Choi, H. (2004). "Behavior and design of structure with buckling-restrained braces." *Eng. Struct.*, 26(6), 693–706.

Krawinkler, H., Zohrei, M., Lashkari-Irvani, B., Cofie, N., and Hadidi-Tamjed, H. (1983). "Recommendations for experimental studies on the seismic behavior of steel components and materials." *John A. Blume Center Rep. No. 61*, Dept. of Civil Engineering, Stanford Univ., Stanford, CA.

Krawinkler, H., (1992). "Guidelines for cyclic seismic testing of components of steel structures." *ATC-24*, Applied Technology Council, Redwood City, CA.

Lanning, J., Benzoni, G., and Uang, C. M. (2011). "The feasibility of using buckling-restrained braces for long-span bridges: A case study." *Rep. No. SSRP 11/09*, Dept. of Structural Engineering, Univ. of California, San Diego, La Jolla, CA.

Lanning, J., Uang, C. M., and Benzoni, G. (2012). "Subassemblage testing of CoreBrace buckling-restrained braces (P Series)." *Rep. No. TR-12/03*, Dept. of Structural Engineering, Univ. of California, San Diego, La Jolla, CA.

Merritt, S., Uang, C. M., and Benzoni, G. (2003). "Subassemblage testing of Star Seismic buckling-restrained braces." *Rep. No. TR-03/04*, Dept. of Structural Engineering, Univ. of California, San Diego, La Jolla, CA.

Moffatt & Nichol Engineers. (1996). "Toll road seismic retrofit project Vincent Thomas Bridge, strategy report." *Rep. to Caltrans*, Caltrans, Sacramento, CA.

Newell, J., Uang, C. M., and Benzoni, G. (2006). "Subassemblage testing of CoreBrace buckling-restrained braces (G Series)." *Rep. No. TR-06/01*, Dept. of Structural Engineering, Univ. of California, San Diego, La Jolla, CA.

PEER (Pacific Earthquake Engineering Research Center). *PEER ground motion database.* Univ. of California, Berkeley, CA. http://ngawest2.berkeley.edu/ (June 1, 2011).

Ravi, K. G., Satish, S. R., and Kalyanaraman, V. (2007). "Behaviour of frames with non-buckling bracings under earthquake loading." *J. Constr. Steel Res.*, 63(2), 254–262.

Richards, P., and Uang, C. (2006). "Testing protocol for short links in eccentrically braced frames." *J. Struct. Eng.*, 10.1061/(ASCE)0733-9445(2006)132:8(1183), 1183–1191.

Romero, P., Reaveley, L., Miller, P., and Okahashi, T. (2007). "Full scale testing of WC series buckling-restrained braces." *Final Rep.*, Dept. of Civil & Environmental Engineering, Univ. of Utah, Salt Lake City, UT.

Sabelli, R., Mahin, S., and Chang, C. (2003). "Seismic demands on steel braced frame buildings with buckling-restrained braces." *Eng. Struct.*, 25(5), 655–666.

Soroushian, P., and Choi, K. B. (1987). "Steel mechanical properties at different strain rates." *J. Struct. Eng.*, 10.1061/(ASCE)0733-9445(1987)113:4(663), 663–672.

Tremblay, R., Bolduc, P., Neville, R., and DeVall, R. (2006). "Seismic testing and performance of buckling-restrained bracing systems." *Can. J. Civil Eng.*, 33(2), 183–198.

Tremblay, R., and Bouatay, N. (2002). "Loading protocols for the seismic testing of ductile bracing members in concentrically braced steel frames." *Proc., 12th European Conf. on Earthquake Eng.*, Elsevier, Oxford, U.K., Paper No. 480.

Usami, T., Lu, Z., and Ge, H. (2005). "A seismic upgrading method for steel arch bridges using buckling-restrained braces." *Earthquake Eng. Struct. Dyn.*, 34(4–5), 471–496.